JOURNAL OF SOLID STATE CHEMISTRY 28, 195–208 (1979)

Dynamic Dielectric Analysis of Solids

R. NOTTENBURG, K. RAJESHWAR,* M. FREEMAN, AND J. DUBOW

Department of Electrical Engineering, Colorado State University, Fort Collins, Colorado 80523

Received February 23, 1978; in revised form July 31, 1978

An automated technique has been developed which enables a rapid determination of the dielectric properties of a material over a wide range of temperatures and frequencies. The speed of data acquisition and the range of temperature and frequencies that can be investigated in a single experiment using this technique, exceed the capabilities of techniques currently employed for dielectric analysis. Frequencies for dielectric measurements can be pre-selected in increments over the range 50 Hz–1 MHz. Temperature range for these measurements extends from 25°C to 800°C. The present technique, which features extensive automation in data acquisition and processing, is illustrated by measurements on minerals and shales. The dynamic nature of the above technique also facilitates effective coupling with conventional thermal analysis techniques.

Introduction

Applications of dielectric analysis techniques in the thermophysical characterization of solids are well documented (*1, 2*). Bridge methods (*3*) that are currently employed for dielectric measurements, are limited by the necessity of using different types of bridges for the various frequency ranges. Another disadvantage of these techniques is the inordinately long time required to make a set of measurements at different temperatures and frequencies. Therefore, a technique which would facilitate a rapid monitoring of the dielectric parameters of a test specimen over a wide range of frequencies and temperatures would be particularly useful for material characterization and routine quality control applications. This paper describes the development of such a technique which we call Dynamic Dielectric Analysis (DDA). The term "dynamic" refers to a continuous scanning over a wide frequency range, typically 50 HZ–1 MHz, and is a major feature of this technique. The speed of data acquisition and the range of frequencies and temperatures that can be studied in a single experiment by DDA, are far beyond the capabilities of conventional bridge methods mentioned above.

The dynamic nature of DDA also makes it readily amenable to coupling with thermal analysis techniques that are based on linear temperature programming like, for example, Differential Thermal Analysis (DTA). The quantitative nature of dielectric techniques, the need for additional techniques to be used in conjunction with DTA for adequate characterization of thermal properties (*4*) and the advantages derived from the application of simultaneous parameter measurement techniques (*5*), point towards the potential applications of simultaneous DTA–DDA in studies on the thermophysical behavior of solids. This is especially true for

* To whom correspondence regarding the manuscript should be addressed.

0022-4596/79/050195-14$02.00/0

complex, heterogeneous systems consisting of naturally-occurring materials on account of the extreme sensitivity of their thermal properties to local compositional variations and to changes in experimental conditions (*6*). Therefore another problem, which also forms the basis of the present paper, was to investigate the applicability of simultaneous DTA–DDA in studies on naturally-occurring materials. Among the systems studied were Green River oil shales, quartz, calcite and dolomite.

Experimental

Techniques

The technique of DDA, developed in the present study uses network analysis techniques to obtain the equivalent passive network components of the test sample. Figure 1 shows a block diagram of the experimental set-up and the data analysis path. A Hewlett-Packard Model 3320B frequency synthesizer provides a sinusoidal signal which is applied both to the sample and the reference channel of the network analyzer. A Hewlett-Packard Model 3570A network analyzer[1] measures the attenuation and phase shift due to the test sample. The network analyzer has a frequency range extending from 50 Hz to 13 MHz. From the attenuation (G) and phase shift (ϕ), an equivalent network is obtained for the test sample. This is shown in Fig. 2. The resulting network equations are derived in Appendix. The dielectric parameters represented by the relative dielectric constant ε', ε'', loss tangent, $\tan\delta$, and resistivity ρ are obtained from the equivalent network and the sample geometry as summarized in Table I. A Hewlett-Packard 9825 desktop computer system is used to record gain and phase (G/ϕ) information and for remote control of the frequency synthesizer and network analyzer.

The sample holder arrangement for DDA is a conventional two-terminal cell similar to that described by Broadhurst and Burr (*7*).

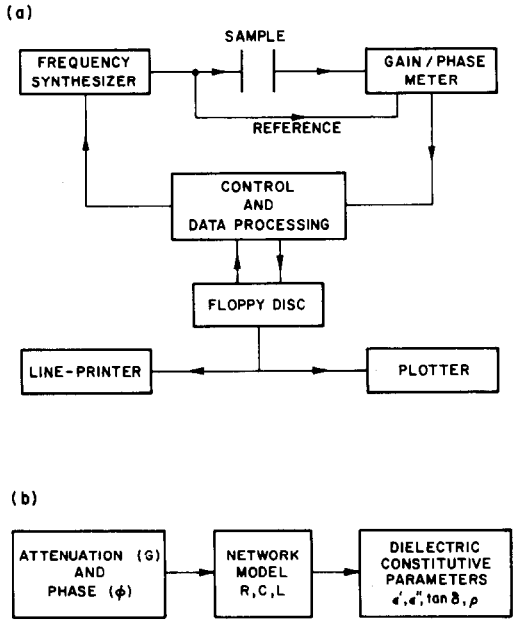

FIG 1(a). A block diagram of the experimental set-up for DDA. (b). Data analysis path in DDA.

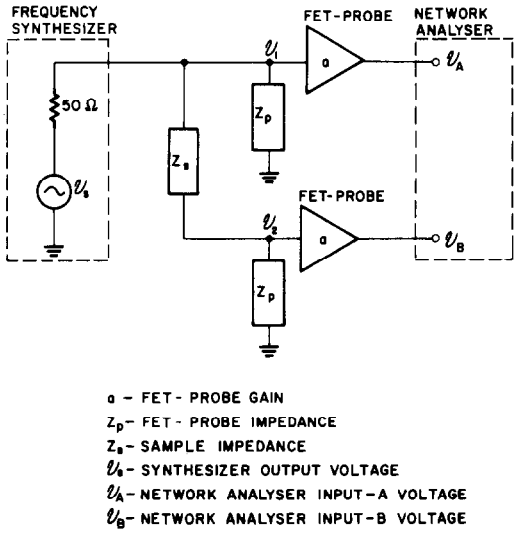

FIG. 2. Equivalent network of the test-sample for DDA.

[1] Reference to a brand name or product does not imply endorsement by the authors or by the funding agencies.

TABLE I

EQUATIONS RELATING ε', ε'', TAN δ AND ρ TO SAMPLE RC COMPONENTS FROM NETWORK ANALYSIS

$\varepsilon' = C_s \frac{d}{A}$	$\varepsilon'' = \frac{\sigma}{\omega}$
$\tan \delta = \frac{\varepsilon''}{\varepsilon'}$	$\rho = \frac{AR_s}{d}$

A = area of sample surface; d = sample thickness; ω = operating frequency; σ = conductivity of sample; C_s = sample capacitance and R_s = sample resistance.

Measurements are carried out on disc-shaped specimens. The test-cell for simultaneous DDA–DTA is shown in Fig. 3 and differs from that employed for DDA only in that a reference sample is included for measurement of differential temperature, ΔT in DTA. The sample cell is housed in a conventional tubular furnace which can be operated either on a linear heating programme or in an isothermal mode. Arrangements are also provided for purging the test-cell with a flowing atmosphere of pre-heated inert gas (usually pre-purified dry N_2). This is particularly useful for the prompt removal of product gases from the vicinity of the heated samples and for avoiding the oxidation of any organic material in the test samples.

The principles of DTA are well-documented in the literature (*8, 9*) and will not be enumerated here.

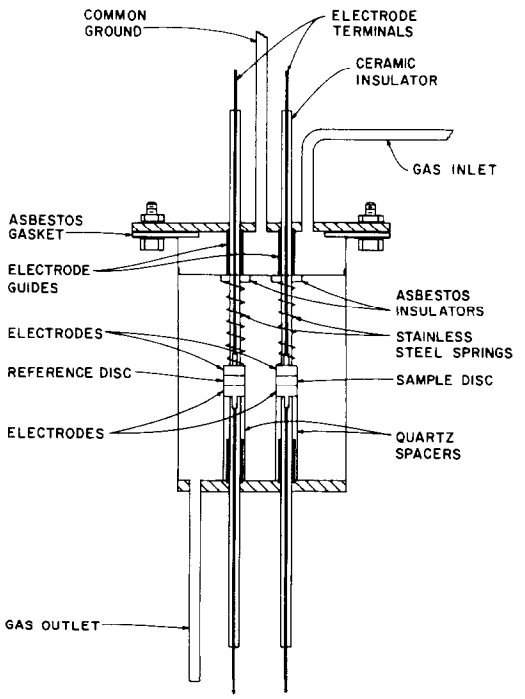

FIG. 3. Test cell for simultaneous DTA–DDA.

Procedure

DDA

The sample is first loaded in the test-cell, care being taken to ensure proper loading of the electrode plates on the sample surfaces. The electrodes are then connected to the frequency synthesizer and network analyzer through high-impedance FET probes. The gas flow is adjusted to obtain a pre-selected flow rate of the sweep gas. The system is thoroughly flushed with the inert gas for about twenty minutes. The heating rate on the temperature programmer is set and the upper temperature limit of the experiment is chosen. The network analysis system is readied for operation by loading the control programs from floppy disc into the 9825 memory. The number of frequency points to be scanned in each decade is pre-selected by the control program. After heating of the test specimen is initiated, a complete frequency spectrum of the G/ϕ values is obtained at preselected temperature intervals. A typical scan time for covering the frequency range 50 Hz–1 MHz is one minute. Low heating rates are generally employed (< 5°C/min) to minimize rapid temperature changes during a frequency sweep. An average of about 25 temperatures are selected for G/ϕ measurements for each DDA run. The number and the frequency of scans are

determined by the thermal behavior of the test specimen and also by the rate of change of G/ϕ values that is observed as a function of temperature. The operator can examine the G/ϕ data being processed by displaying the results on a CRT terminal or other output devices. G/ϕ results from each individual frequency scan are recorded as a function of temperature on floppy discs. Data is organized into files on these discs for reduction by automatic analysis programs.

Simultaneous DDA–DTA

Reference alumina discs are included for simultaneous DDA–DTA measurements and ΔT is continuously monitored as a function of time or temperature on a strip-chart or x–y recorder. As mentioned above, it is necessary to employ low heating rates for these measurements. Very low heating rates, of course, give rise to DTA peaks high in resolution but weak in intensity (*10*). A compromise is, therefore, sought between the minimum sensitivity that can be tolerated for DTA and the highest heating rate that can be employed for DDA. A heating rate of ~3°C/min has been found to yield good results for simultaneous DDA–DTA with the system described above. The relatively thin specimens and low heating rates also serve to minimize thermal gradients across the samples (*11*). Temperature intervals for DDA during a DTA scan are preselected; G/ϕ measurements being carried out more frequently during a temperature region of interest like a thermal decomposition or phase transformation as shown in Fig. 4.

Data Acquisition and Processing

Data acquisition for DDA is completely automated; computer programs[2] have been developed in this laboratory for conversion of raw experimental G/ϕ data to dielectric parameters that can be directly correlated

[2] All programs are written in HPL language. Copies of control and data analysis programs are available from the authors on request.

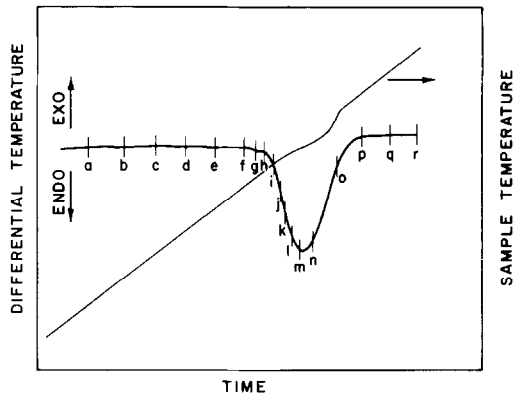

FIG. 4. Measurement intervals for DDA during a DTA scan in simultaneous DTA–DDA. (Points a, b, c, d . . . , represent successive G/ϕ scans as a function of frequencies in the range 50 Hz–1 MHz.)

with work previously reported in the literature. The parameters ε', ε'', $\tan\delta$ and ρ as functions of frequency and temperature are either printed out on a line-printer or plotted on a Hewlett-Packard Model 9872 digital plotter.

The type of information that can be obtained on the thermal and electrical properties of the test specimen from DDA and simultaneous DDA–DTA measurements, is summarized in Table II.

Sample Preparation

Oil shale samples used in the present study were obtained in mine-fresh condition from the Paraho Oil Shale Development Corporation, Rifle, Colorado, and from the LERC, Laramie, Wyoming. Oil contents of the shale samples were determined by specific gravity measurements using correlation tables (*12*). Care was taken to select samples which were crack-free. Samples of natural Brazilian quartz, dolomite (Colorado, U.S.A.) and calcite (Utah, U.S.A.) were obtained from commercial sources. Right-circular cylindrical cores measuring $\frac{7}{8}$ in. Diameter, $\frac{1}{8}$ in. thick and drilled from massive blocks of the starting material were used for measurements on the various samples. Data reproducibility was

TABLE II

MEASURED PARAMETERS AND THE TYPE OF INFORMATION OBTAINED IN DDA AND DTA

DDA		DTA	
Measured parameter[a]	Type of information	Measured parameter[a]	Type of information
$\varepsilon'(\omega, T)$[b] $\varepsilon''(\omega, T)$ $\tan \delta(\omega, T)$ $\rho(\omega, T)$	Dispersion behavior, changes in dielectric parameters during a chemical or physical change, activation energy for dipole orientation, activation energy for current carrier mobility	$\Delta T(t, T)$ $T_s(t, T)$ $T_R(t, T)$	Nature of thermal effect, phase transition behavior, nature of heat effect (whether exothermic or endothermic), non-isothermal kinetics, semi-quantitative ΔH values

[a] ω = frequency, T = temperature, t = time, T_s = temperature of sample, T_R = temperature of reference, $\Delta T = T_s - T_R$.

[b] The parameters in parentheses denote experimental variables.

checked by coring sets of samples from the same block and with identical varve structure and organic content in the case of shales. All samples were carefully dried to remove free moisture and stored in vacuum prior to measurements.

Error Analysis and Data Reproducibility

Errors inherent in DDA and simultaneous DDA–DTA measurements are twofold: (a) instrumental, and (b) those arising from samples.

The performance of the test set-up for DDA was checked with standard capacitor and resistor components combined in parallel. Table III summarizes the range of values in ε', ε'', ρ, and tan δ that is usually measured and the associated errors in their measurement.[3] A more detailed analysis of the measurement network will be reported elsewhere (*13*). Stray capacitance effects were automatically accounted for in the experimental results from "dummy" measurements carried out with air-gap between the electrodes. Good electrical contact between the sample surface and the electrodes was ensured by appropriate loading of the electrode contact plates. Silver paint was employed in a few experiments to

[3] It must be pointed out that the error analysis presented in Table III does not take into account measurement errors arising from extraneous capacitance effects in the sample holder assembly.

TABLE III

RANGE OF TAN δ VALUES AND ERRORS IN THE MEASUREMENT OF ε', ε'', TAN δ AND ρ DUE TO THE NETWORK ANALYZER[a] FOR MIDBAND FREQUENCY, 10 kHz

Sample tan δ	± % Error ε'	± % Error ε''	± % Error tan δ	± % Error ρ
300	100	1.5	100	1.5
30	15	1.3	18.0	1.3
3.0	1.5	1.0	3.0	1.0
0.3	0.5	1.0	1.5	1.0
0.03	0.4	5.0	6.0	5.0

[a] Using gain linearity ±0.01 *dB* near 0 *dB* and phase linearity ±0.02° near 0°.

reduce contact resistance but subsequent investigation proved this effect to be negligible. Electrode effects were checked by comparing results of measurements with different electrode materials; no noticeable effect was found. Subsequent measurements were carried out with electrodes and lead wires made of silver.

Additional scatter in the dielectric data arises from local composition variations in the test specimens. In the case of oil shales, minor differences in their sedimentary varve structure were found to give rise to mean sample-to-sample deviations in the results ranging from ±6% for the leaner shales to ±3% for shales with high organic content. Such variations are found to be small for the samples of quartz, dolomite and calcite examined in the present study and attest to the relatively homogeneous nature of these materials.

Calibration

Capacitance measurements using DDA were calibrated using potassium bromide, potassium chloride and sodium chloride. Single crystalline discs of these materials of ultra-high purity were obtained from commercial sources. Values obtained for $\varepsilon'/\varepsilon_0$ in the present study were compared with those reported in the literature for these materials (*14*). Typical calibration results are shown in Table IV.

TABLE IV

TYPICAL CALIBRATION RESULTS FOR DDA

Material	Frequency range	Measured $\varepsilon'/\varepsilon_0$	Reported[a] $\varepsilon'/\varepsilon_0$ (Ref. *14*)
NaCl	10^2–10^5	5.90±0.05	5.90
KCl	10^2–10^5	4.84±0.10	4.84
KBr	10^2–10^6	4.94±0.05	4.90

[a] The nominal accuracies reported for the $\varepsilon'/\varepsilon_0$ values of the various materials in Ref. 14 are ±2%.

Temperature calibration for DTA was checked with samples of ammonium nitrate, benzoic acid, potassium perchlorate, and calcium oxalate monohydrate. Peak temperatures obtained for the various thermal transformations in these materials show close agreement with published results (*15, 16*). DTA curves for the above samples obtained with the apparatus described above are shown in Figs 5 and 6. The precision of the temperature measurement corresponding to a DTA peak is estimated to be ±2%.

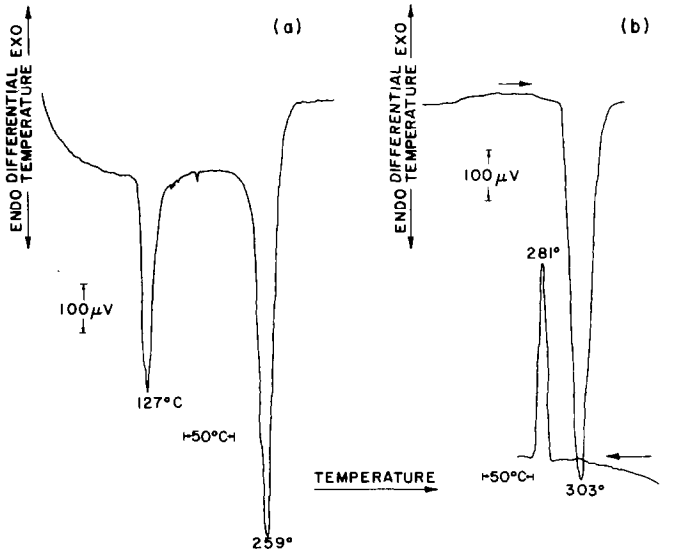

FIG. 5. DTA curves for (a) benzoic acid, and (b) potassium perchlorate. (Heating rate 5°C/minute, flowing nitrogen atmosphere. Cooling rate in (b) uncontrolled.)

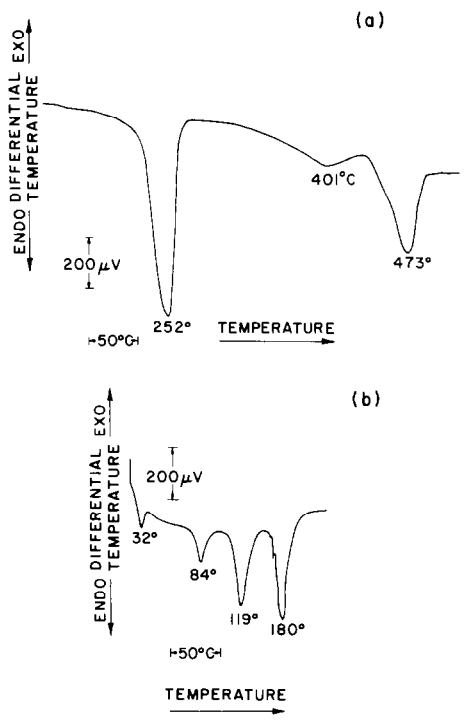

FIG. 6. DTA curves for (a) calcium oxalate monohydrate, and (b) ammonium nitrate. (Heating rate 5°C/minute; flowing nitrogen atmosphere.)

Results and Discussion

Figure 7 shows DDA results on the room-temperature dielectric behavior of dolomite, calcite and quartz; the frequency dependence of the relative dielectric constant ε' is compared with results reported in the literature on these materials. ε' is seen to exhibit non-dispersive behavior for all the mineral samples examined in the present study. The pronounced dispersion effects reported for dolomite (Brewster, New York) in a previous study (*17*) are to be noted. On the other hand, none of the dolomite samples in the present investigation show pronounced variations in ε' with frequency. It is possible that variations in the chemical composition and/or minor differences in depositional history in the two cases, could explain this difference in the dielectric behavior of dolomite. The chemical composition of the dolomite samples is not reported in the aforementioned study (*16*) and this precludes a direct comparison of the data obtained in the two studies. It is significant, however, that ε' values reported

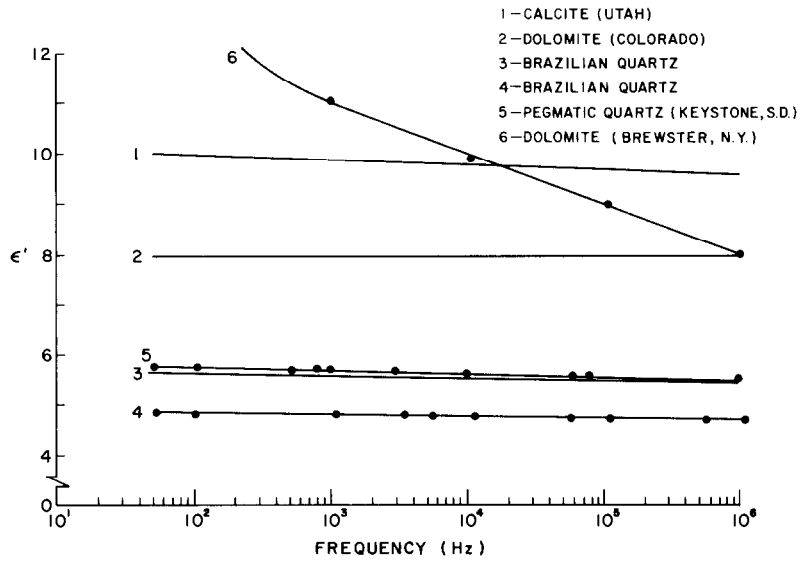

FIG. 7. Variation of ε' with frequency at 25°C for calcite, dolomite and quartz. (Data in curves 4, 5 and 6 are from Ref. *16*).

by Howell and Licastro (*17*) at high frequencies (>1 MHz) coincide with those observed in the present investigation (Fig. 7). Values of ε' for calcite and quartz are also in good agreement with results reported in the literature (*17, 18*).

Figures 8 and 9 are representative DTA curves on Green River oil shales obtained with the apparatus described above. These DTA results were obtained simultaneously with DDA on the same test specimens (see below). The thermal decomposition of the shale organic matter is seen to be endothermic and takes place in the range 400–500°C. Minor variations are observed in the DTA peak temperatures depending on the source and type of the shales. The splitting of the endothermic peaks in Figs 8 and 9 seems to indicate that the thermal decomposition of organic matter in the shale is a multistep process. Thermal degradation of the shale hydrocarbons followed by distillation of the various fractions from the residue in a sequencial manner is expected to give rise to overlapping endothermic behavior in DTA. The small peak at ~352°C in Fig. 8 is attributed to the thermal decomposition of analcite, initially present in the shale. This assignment is consistent with previous studies on the thermal behavior of analcite (*19*).

Typical DDA data showing the variation of dielectric parameters with frequency at 25°C are shown in Table V for a 37 gallons/ton oil shale sample. ε' is seen to exhibit frequency dependence characteristics of other water-bearing sedimentary rocks and minerals (*20*)—a sharp decrease in ε' at low frequencies and a very gradual decreasae with increasing frequency at higher frequencies. Variations in ε' values of Green River oil shale with temperature in the frequency range 10 Hz–1 MHz are shown in Figs 10 and 11. The high ε' values observed at low frequencies are attributed to strong Maxwell–Wagner interfacial polarization effects arising from the presence of varve boundaries in the material (*21*). The initial decrease in ε' with temperature (Fig. 10) followed by a subsequent increase at higher temperatures (Fig. 11) is correlated with the effect of release of pore water from the shale matrix and the presence of amorphous carbon in the shale residue arising from the decomposition of the organic matter respectively (*21*).

The data in Table V also reveal a sharp increase in the electrical conductivity of oil

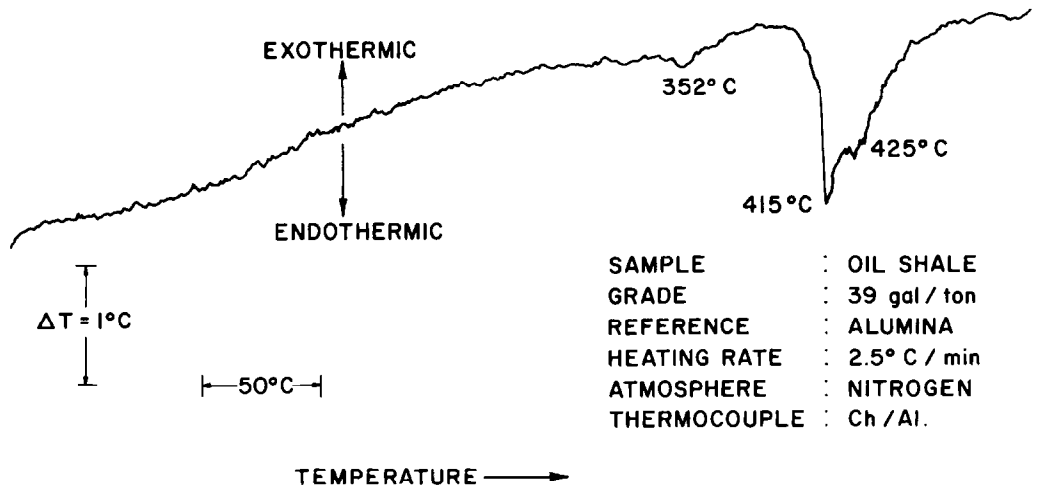

FIG. 8. DTA curve for a 39 gallons/ton Green River oil shale sample.

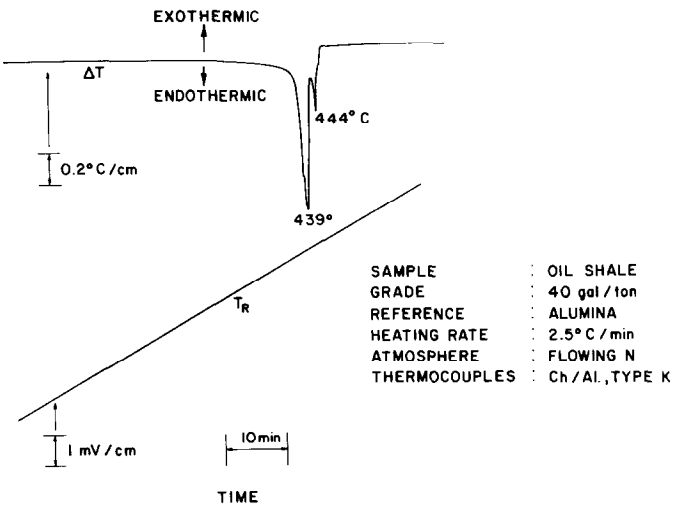

FIG. 9. Time-based DTA record of a Green River oil shale sample.

shale with increasing frequency. This behaviour is consistent with previously published work on sedimentary materials like limestone and marl (*20*); which shows that the lower the water content and/or the lower the conductivity of the mineral, the greater is the increase in conductivity with increasing frequency. Pore water content of oil shale is variable; however, it seldom exceeds 6–10%, which is well within the limits observed for sedimentary rocks which exhibit similar dielectric behavior.

The nature of dispersion in tan δ for a 26 gallon/ton shale sample is typically as shown in Fig. 12. Similar behavior is observed for other shales with varying organic content. The presence of a broad peak in tan δ at frequencies below 100 Hz is strongly indicative of interfacial polarization behavior (*22*). The occurrence of secondary maxima in tan δ at higher frequencies, which is only observed at temperatures above ~450°C is also to be noted. These tan δ peaks are correlated with dipole relaxation effects arising from the thermal decomposition of the shale organic matter. The close correspondence of the temperatures at which these peaks occur with the DTA peak temperatures for oil shale in Figs 8 and 9, provides additional evidence for this hypothesis. Splitting-off of the polar segments from the giant macromolecular network in the organic

TABLE V

DIELECTRIC ANALYSIS OF GREEN RIVER OIL SHALE AT 25°C

Frequency (Hz)	Resistivity (ohms-cm)	Capacitance (Farads)	ε'	ε''	tan δ	A.C. conductivity (mho-cm^{-1})
100	0.236×10^{10}	0.164×10^{-10}	18.91	0.77	0.041	0.432×10^{-10}
1000	0.480×10^{9}	$0{\cdot}150\times10^{-10}$	17.21	0.38	0.022	0.212×10^{-9}
4000	0.369×10^{8}	0.142×10^{-10}	16.28	1.24	0.076	0.276×10^{-8}
10000	0.963×10^{7}	0.134×10^{-10}	15.35	1.90	0.124	0.106×10^{-7}
52000	0.113×10^{7}	0.108×10^{-10}	12.39	3.11	0.251	0.102×10^{-6}
94000	0.808×10^{5}	0.522×10^{-11}	6.35	2.41	0.380	0.126×10^{-5}

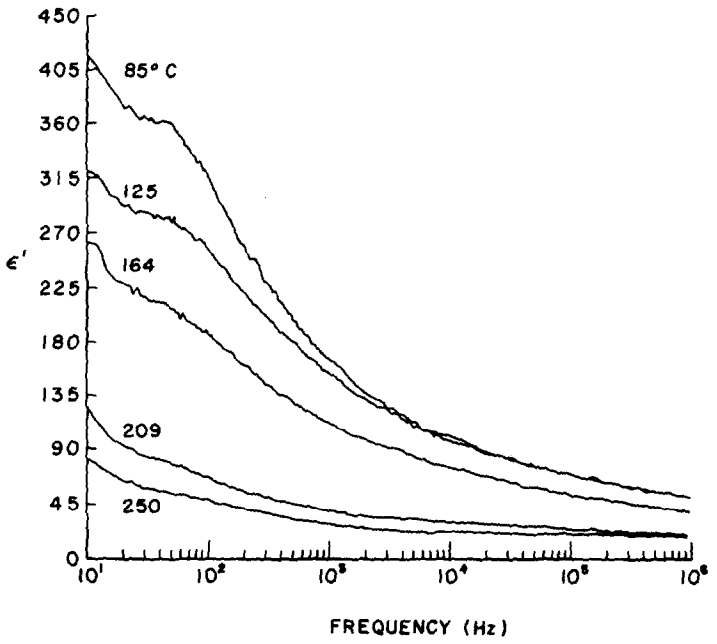

FIG. 10. Variation of ε' with frequency for Green River oil shale at low temperatures (< 250°C).

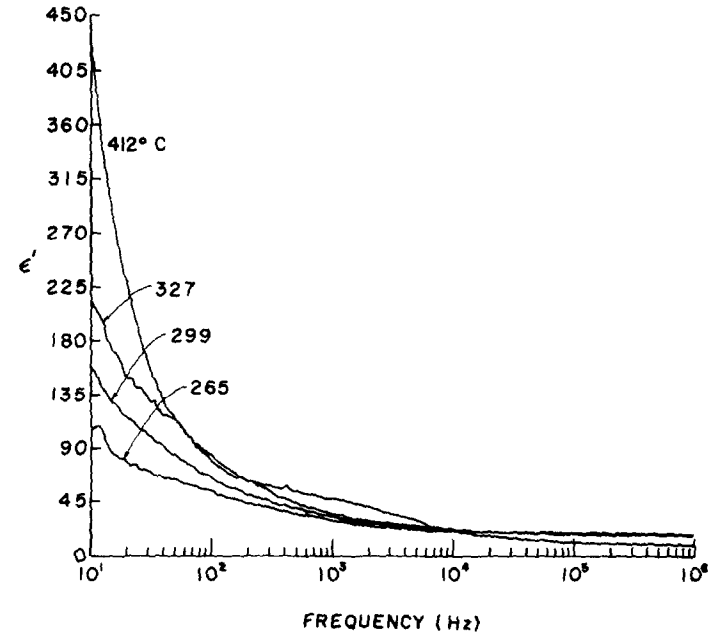

FIG. 11. Variation of ε' with frequency for Green River oil shale at high temperatures (>250°C).

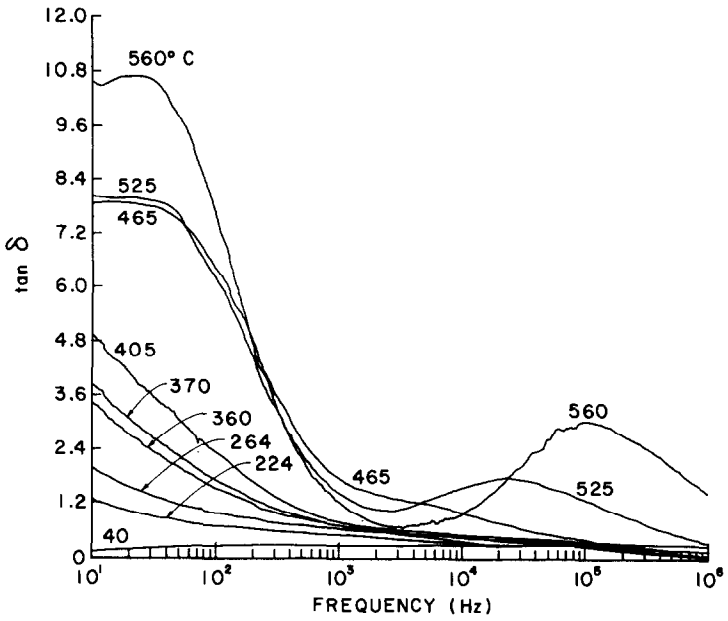

FIG. 12. Dispersion in tan δ for a 26 gallons/ton oil shale sample at different temperatures.

matric (*23*) as a result of thermal fragmentation, presumably brings about a change in their rotational freedom with a resultant change in their polarizability. Further support for this interpretation is given by the pronounced dependence of tan δ peaks on temperature in Fig. 12. These peaks shift to higher frequencies with increasing temperature as expected from the well-known equation (*24*)

$$\nu_{max} = \frac{1}{2\pi\tau_0} \frac{\varepsilon_\infty + 2}{\varepsilon_0 + 2} \exp\left(-\frac{E_d}{kT}\right) \qquad (1)$$

where ν_{max} = frequency corresponding to the peak in tan δ, τ_0 = dipole relaxation time, ε_∞ = permittivity at optical frequencies, ε_0 = static dielectric constant, E_d = activation energy for dipole orientation, k = Boltzmann constant, and T = absolute temperature. A plot of log ν_{max} versus $1/T$ should therefore yield a straight line on the basis of the above model; Fig. 13 illustrates this behavior for a 26 gallon/ton shale. Similar results for shales with varying organic content confirm the validity of a classical Debye model (*25*) for the dielectric properties of Green River oil shales at temperature corresponding to the decomposition of the organic matter.

The results discussed for Green River oil shale illustrate the utility of simultaneous DTA and DDA measurements. Loss of pore water from the shale matrix, while clearly evident in the dielectric data obtained by DDA (Fig. 10 and 11), is not shown by the

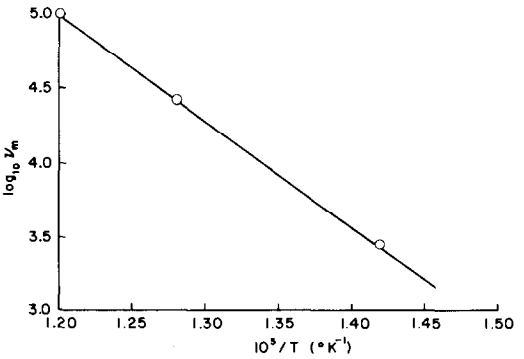

FIG. 13. Plot of log ν_{max} versus $1000/T$ for the sample in Fig. 12.

DTA curves[4] (Fig. 8 and 9). On the other hand, interpretation of the pronounced changes observed in the various dielectric parameters at elevated temperatures (cf. Fig. 11 and 12) is considerably simplified by supplementary information obtained from a simultaneous DTA experiment. Another aspect of the complimentary nature of the two techniques is clearly illustrated in the electrical resistivity-temperature plot shown in Fig. 14 for a 36 gallons/ton shale sample. The DDA results in Fig. 14 were obtained on samples heated in an isothermal mode; resistivity values being measured at each temperature stabilized to ±1°C and with sufficient "settling-time" at each frequency. The broad minima in the resistivity curves in the range 25°–350°C arise from the effect of release of pore water discussed above. Absence of such minima in the curves for the reheated shale samples confirms their origin. More significant, however, are the sharp peaks in the resistivity at ~380°C. Abrupt changes in the mechanical properties of the shale which have been observed at this temperature (*26*), point towards the occurrence of a structural transition preceding the thermal decomposition of the organic matter in the shale. DTA curves (Figs 8 and 9) on the other hand do not show any significant thermal effect corresponding to this transition. Therefore an examination of the DTA curves alone would have given an incomplete picture of the thermophysical behavior of the test specimen.

In addition to the aforementioned advantages of simultaneous DDA–DTA, another important factor, especially in routine material characterization is the considerable savings in time gained by simultaneous techniques. Exposure of test samples to identical experimental conditions also facilitates a direct comparison of the trends observed in their thermal and electrical properties.

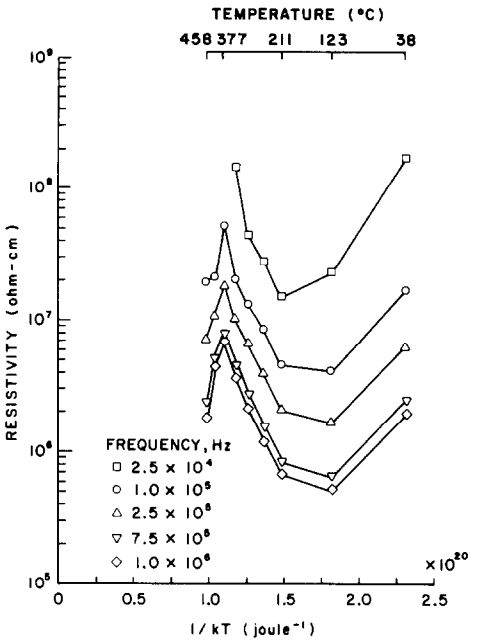

FIG. 14. Electrical resistivity versus $1/kT$ for a 36 gallons/ton shale sample at different frequencies.

It must be pointed out that the techniques developed in the present study are applicable to inorganic and organic solids in general. Changes in dielectric parameters during a solid-state transformation can be conveniently studied by DDA and simultaneous DDA–DTA. Application of these techniques to polymeric systems is also another interesting possibility.

Conclusions

An automated technique has been developed which enables a rapid monitoring of the dielectric properties of a material over a wide range of temperatures and frequencies. The dynamic nature of this technique

[4] The temperature range in which pore water and adsorbed water are driven off from the oil shale matrix is quite broad, viz ~25–350°C. This results in the absence of well-defined endothermic peaks in the DTA, corresponding to the loss of pore water and adsorbed moisture. The gradual weight loss observed in the thermogravimetric curves for Colorado oil shales at these temperatures [by previous investigators, (*27*)] also essentially conforms to the trends in the corresponding DTA behavior observed in the present study.

enables its effective coupling with conventional thermal analysis techniques like DTA. Application of the technique developed in the present study to studies on naturally-occurring materials, illustrates their usefulness in an adequate characterization of thermophysical behavior.

Acknowledgments

This research program was carried out with financial support from NSF/RANN Grant AER75-18650 and Laramie Energy Research Center Grant E-(29-2)-3564. The authors would also like to thank Mr. P. J. Singh for help in the calibration experiments.

Appendix

The FET Probe gain $a \equiv a(s)$ is slightly frequency dependent, and its effect is effectively cancelled by using two probes into the network analyzer to determine the complex gain

$$\frac{\mathcal{V}_2}{\mathcal{V}_1} = \frac{a(s)\mathcal{V}_B}{a(s)\mathcal{V}_A} = \bar{G}$$

The gain is calculated from the voltage-divider expression (ignoring source resistance).

$$\bar{G} = \frac{Z_p}{Z_p + Z_s} \tag{1}$$

Solving for Z_s gives:

$$Z_s = Z_p \frac{1-\bar{G}}{\bar{G}} \tag{2}$$

which in polar form is:

$$|Z_s| \equiv \kappa = \frac{|Z_p| \cdot |1-\bar{G}|}{|\bar{G}|} \tag{3}$$

$$\angle Z_s \equiv \phi = \angle Z_p + \angle(1-\bar{G}) - \angle\bar{G} \tag{4}$$

The right-hand side values must be determined.

$\angle\bar{G}$ and $|\bar{G}|$ in dB are found directly from the network analyzer.

$$|1-\bar{G}| = \sqrt{1-2A\cos\theta + A^2} \tag{5}$$

$$\angle(1-\bar{G}) = -\tan^{-1}\left(\frac{\sin\theta}{1/A - \cos\theta}\right) \tag{6}$$

where $A \equiv |\bar{G}|$, $\theta \equiv \angle\bar{G}$.

The FET-Probe input impedance Z_p can be modeled as a parallel resistance and capacitance.

$$|Z_p| = \frac{R_p}{\sqrt{1+(\omega R_p C_p)^2}} \tag{7}$$

$$\angle Z_p = -\tan^{-1}(\omega R_p C_p) \tag{8}$$

where R_p is the input resistance and C_p is the input capacitance and ω is the angular frequency: $\omega = 2\pi f$.

The equivalent resistance and capacitance of the sample (R_s, C_s) can be determined from Eqs (3) and (4) by the relations:

$$R_s = \kappa \sec\phi$$

$$C_s = -\frac{1}{\omega\kappa}\sin\phi$$

References

1. J. B. Birks and J. Hart, (Ed.) "Progress in Dielectrics," Vol. 3. Wiley, New York (1961).
2. P. Hedvig, "Dielectric Spectroscopy of Polymers," Wiley, New York (1977).
3. N. E. Hill, W. E. Vaughan, A. H. Price, and M. Davies, "Dielectric Properties and Molecular Behavior," Chap. 2, p. 108, Van Nostrand-Reinhold, New York (1969).
4. W. W. Wendlandt, "Thermal Methods of Analysis," 2nd ed. Chapt. 11, p. 428. Wiley, New York (1974).
5. J. W. Smith and D. R. Johnson, *in* "Thermal Analysis," Vol. 1, p. 1251, (R. F. Schwenker Jr. and P. D. Garn Eds.) Academic Press, New York (1969).
6. J. W. Smith in "Thermal Analysis," Vol. 3 p. 605 (H. G. Wiedemann Ed.), Birkhaüser-Verlag (1972).
7. M. G. Broadhurst and A. J. J. Burr, *Res. Natn. Bur. Stand.* 69C, 165 (1965).

8. M. I. POPE AND M. D. JUDD, "Differential Thermal Analysis," Heyden, London (1977).
9. W. J. SMOTHERS AND Y. CHIANG, "Differential Thermal Analysis, Theory and Practice," Chemical Publishing Co. (1958).
10. A. BLAZEK, "Thermal Analysis," Chap. 3, p. 94. Van Nostrand-Reinhold, New York (1972).
11. P. D. GARN, "Thermoanalytical Methods of Investigation," Chap. 2, p. 23, Academic Press, New York (1965).
12. J. W. SMITH, U. S. Bureau of Mines, Rept. 7248, 14 pp. (1969).
13. R. NOTTENBURG, M. FREEMAN, K. RAJESHWAR, AND J. DUBOW, to be published.
14. A. VON HIPPEL, (Ed.) "Dielectric Materials and Application," Technology Press of MIT and Wiley, New York (1954).
15. K. RAJESHWAR AND V. R. PAIVERNEKER, *Thermochim. Acta* **13**, 293, (1976).
16. Reference 10, p. 42, Reference 4, p. 261.
17. B. F. HOWELL, JR. AND P. H. LICASTRO, *Amer. Mineral.* **46**, 269, (1961).
18. S. P. CLARK, JR., Editor, "Handbook of Physical Constants," Revised Edition, p. p. 569, Section 26, Geological Society of America (1966).
19. D. R. JOHNSON, N. B. YOUNG AND W. A. ROBB, *Fuel* (London) **54**, 249, (1975).
20. E. I. PARKHOMENKO, "Electrical Properties of Rocks," Chap. 4, p. 200, Plenum Press, New York (1967).
21. K. RAJESHWAR, R. N. NOTTENBURG, R. J. ROSENVOLD AND J. B. DUBOW, *Thermochim. Acta.* **27**, 357 (1978).
22. J. B. HASTED, "Aqueous Dielectrics," p. 238, Chapman and Hall, London (1973).
23. T. F. YEN in "Science and Technology of Oil Shale," Chap. 7, p. 130. (T. F. Yen Ed.) University of Michigan, Ann Arbor (1975).
24. P. HEDVIG AND G. ZENTAI, "Microwave Study of Chemical Structures and Reactions," (English translation E. D. Morgan Ed.), p. 122, Illiffe Books, London (1969).
25. H. FRÖHLICH, "Theory of Dielectrics," Second Edition, Chap. 3, p. 70, Clarendon Press, Oxford (1958).
26. R. NOTTENBURG, K. RAJESHWAR, R. ROSENVOLD, AND J. DUBOW, *Fuel*, in press.
27. A. *27.* A. Y. HERRELL AND C. ARNOLD, Jr., *Thermochim. Acta* **17**, 165 (1976).